

## MODELLING AND ANALYSIS TOOLS FOR INTERFEROMETRIC SAR OBSERVATIONS

M. Crosetto <sup>a</sup>, B. Crippa <sup>b</sup>, R. Barzaghi <sup>c</sup>, M. Agudo <sup>a</sup>

<sup>a</sup> Institute of Geomatics, Campus de Castelldefels, 08860 Castelldefels (Barcelona), Spain  
michele.crosetto@ideg.es, marta.agudo@ideg.es

<sup>b</sup> Department of Earth Sciences, University of Milan, Via Cicognara 7, 20129 Milan, Italy  
bruno.crippa@unimi.it

<sup>c</sup> DIAR, Politecnico di Milano, P. Leonardo da Vinci 32, 20133 Milan, Italy  
riccardo@geo.polimi.it

Commission II, WGII/2

**KEY WORDS:** SAR, Monitoring, Modelling, Estimation, Simulation.

### ABSTRACT:

A quantitative deformation monitoring using the differential interferometric SAR (DInSAR) technique may be achieved when multiple DInSAR observations and suitable modelling and analysis tools are employed. The paper begins with a description of the main characteristics of the DInSAR data. Then, it discusses a new modelling and filtering strategy, which takes advantage of the specific properties of the DInSAR observations. The core of the procedure is the least squares collocation filtering and prediction, which exploits the correlation properties of the DInSAR data. The proposed procedure was tested on simulated DInSAR data that reproduce the characteristics of a small scale and slow deformation rate subsidence, and that include the main components of the interferometric data: the atmospheric contribution, the phase noise component, and the outliers due to the unwrapping related errors.

### 1. INTRODUCTION

The differential interferometric SAR technique (DInSAR), based on spaceborne SAR data, has been successfully employed in different application fields: glacier dynamics (Goldstein et al., 1993; Kwok and Fahnestock, 1996); earthquakes (Massonnet et al., 1993; Massonnet et al., 1994); volcanoes (Massonnet et al., 1995; Amelung et al., 2000); landslides (Carnec et al., 1996); and the deformations related to water resource exploitation, mining activity, and construction works (Amelung et al., 1999). The above applications require different quality levels to the estimates provided by DInSAR. A quite qualitative use of the DInSAR results seems to be sufficient for the purposes of some applications. This is the case of several studies where the geophysical interpretation may be simply based on the qualitative information derived from DInSAR observations, see Tesauro et al. (2000) and Lu and Danskin (2001). However, this is not the case for some other important applications, e.g. the subsidence monitoring in urban areas, which need to be characterised by high quality standards like those usually achieved by the geodetic techniques. This type of applications need a fully quantitative DInSAR monitoring based on multiple observations (multiple interferograms) of the phenomenon under analysis.

The DInSAR technique may provide a quantitative monitoring tool only if suitable data modelling and analysis procedures are employed. It is important to note that the use of multiple DInSAR observations requires 3D modelling and data analysis tools. In literature these procedures have received little attention. Furthermore, little importance has been usually given to important quality aspects, like the precision, accuracy and reliability of the DInSAR estimates. Berardino et al. (2001) describe a procedure to combine multiple interferograms, which works pixelwise connecting the observations of a single pixel with a 1D model. Ferretti et al. (2000) also adopt a 1D model,

which is coupled with a spatially smoothing filter. Other authors, like Strozzi et al. (2001) and Williams et al. (1998), simply compute the average of multiple interferograms (interferogram stacking).

This paper describes new modelling strategies based on 2D and 3D adaptive models (the discussed results concern the 2D case), which fully take advantage of the specific properties of the DInSAR observations. This work only focuses on phenomena characterized by vertical displacements. The paper begins with a description of the basic properties of the DInSAR observations. This is followed by the discussion of a modelling strategy for multiple DInSAR observations and the results obtained on 3D simulated datasets. Section four describes some possible evolutions of the described research.

### 2. CHARACTERISTICS OF THE DINSAR DATA

The D-InSAR technique exploits the phase difference (interferometric phase)  $\Delta\Phi_{Int}$  of two SAR images (hereafter referred to as the master -  $M$  - and the slave -  $S$  - images). Let us consider a point  $P$  on the ground, which remains stable in the time interval between the image acquisitions.  $\Delta\Phi_{Int}$  is related to the distance difference  $SP - MP$ , which is the key element for the InSAR DEM (Digital Elevation Model) generation. When the point moves from  $P$  to  $P^1$  between the two image acquisitions, besides the phase component due to terrain topography,  $\Phi_{Topo}$ ,  $\Delta\Phi_{Int}$  includes the terrain movement contribution,  $\Phi_{Mov}$ . In the general case  $\Delta\Phi_{Int}$  consists of the following components:

$$\Delta\Phi_{Int} = \Phi_S - \Phi_M = \frac{SP - MP}{4 \cdot \pi} + \frac{SP^1 - SP}{4 \cdot \pi} + \Phi_{Atm} + \Phi_{Noise} =$$

$$= \Phi_{Topo} + \Phi_{Mov} + \Phi_{Atm} + \Phi_{Noise}$$

where  $\Phi_S$ ,  $\Phi_M$  are the phases of  $S$  and  $M$ ;  $\Phi_{Atm}$  is the atmospheric contribution;  $\Phi_{Noise}$  is the phase noise;  $SP^1$  is the slave-to-  $P^1$  distance; and  $\lambda$  is the radar wavelength. If the terrain topography is known (i.e. a DEM of the imaged area is available),  $\Phi_{Topo}$  can be computed ( $\Phi_{Topo\_Sim}$ ) and subtracted from  $\Delta\Phi_{Int}$ , obtaining the D-InSAR phase  $\Delta\Phi_{D-Int}$ :

$$\Delta\Phi_{D-Int} = \Delta\Phi_{Int} - \Phi_{Topo\_Sim} = \Phi_{Mov} + \Phi_{Atm} + \Phi_{Res\_Topo} + \Phi_{Noise}$$

where  $\Phi_{Res\_Topo}$  represents the residual component due to DEM errors. In order to derive information on the terrain movement,  $\Phi_{Mov}$  has to be separated from the other phase components. When multiple DInSAR observations are available, the following important properties may be exploited to this purpose (see next section):

1.  $\Phi_{Mov}$  is highly correlated, spatially and temporally;
2.  $\Phi_{Atm}$  is correlated spatially, and uncorrelated temporally;
3.  $\Phi_{Noise}$  and  $\Phi_{Res\_Topo}$  can be considered spatially decorrelated (hereafter they are referred to as the noise). As far as  $\Phi_{Res\_Topo}$  is concerned, this assumption holds for high quality DEMs, e.g. the high resolution photogrammetric DEMs, while it does not hold for the InSAR DEMs, potentially affected by atmospheric effects.

It is important to underline that the above properties can only be exploited when multiple DInSAR observations are available, i.e. when a 3D sampling of the subsidence phenomenon under analysis is performed: 2D in space, plus the time. Using a single interferogram it is in principle not possible to separate  $\Phi_{Mov}$  from the other phase components, in particular from  $\Phi_{Atm}$ : this fact represents an important limitation of the DInSAR technique. An exception occurs dealing with small-scale subsidences, when a priori information on the subsidence area is available (Crosetto et al., 2002a). The key step is the identification of stable areas in the vicinity of the deformation area under analysis. On those areas  $\Phi_{Mov}$  is naught: it is therefore possible estimate  $\Phi_{Atm}$ , which represents the only spatially correlated component (signal) of  $\Delta\Phi_{D-Int}$ .  $\Phi_{Atm}$  can be estimated by analysing the spatial autocorrelation of  $\Delta\Phi_{D-Int}$ . We base this analysis on the autocovariance function, whose characteristic parameters are the variance of the signal  $\sigma_S^2$  and the correlation length  $L_C$ . An interferogram weakly affected by atmospheric effects will be characterised by a nearly zero value of  $\sigma_S^2$  and  $L_C$ , while in presence of atmospheric heterogeneities the two parameters will be significantly different from zero. The above criterion can be used to classify reliable and potentially degraded interferograms. The autocovariance functions of the phase of three ERS-1/2 interferograms, which were computed over a 3 by 2 km stable

area, are shown in Figure 1. One may notice the different behaviour of the two interferograms affected by strong atmospheric components, Int2 and Int3, and Int4, which is characterized by a weak  $\Phi_{Mov}$ . Over the stable areas  $\Phi_{Atm}$  can be separated from the other two components (filtering). Moreover, it can be predicted over the subsidence area and subtracted from the original phase  $\Delta\Phi_{D-Int}$ , hence reducing the atmospheric effects. For a detailed description of the procedure, which is based on the method of the least squares (LS) collocation, see (Crosetto et al., 2002a).

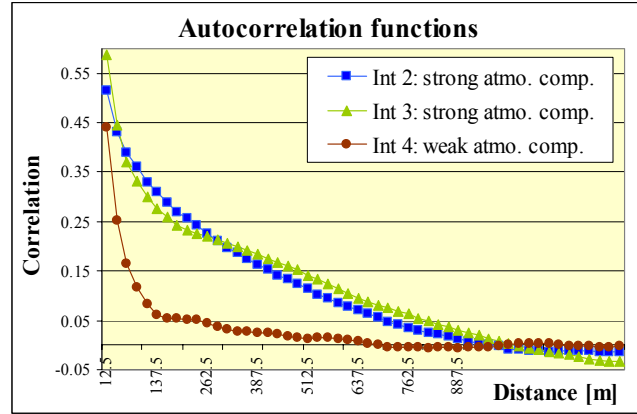


Figure 1. Autocovariance functions of the phase of three ERS-1/2 interferograms, computed over a 3 by 2 km stable area.

### 3. A 2.5D MODELLING FOR MULTIPLE DINSAR OBSERVATIONS

The fusion of multiple DInSAR observations involves a 3D modelling of the subsidence at hand: two dimensions in space, plus the time. As already mentioned in the introduction, the models proposed in literature are sometimes only limited to one single dimension of the phenomenon under analysis, see the 1D models adopted by Bernardino et al. (2001) and Ferretti et al. (2000): they provide a pointwise description of the subsidence temporal evolution. Other authors employ a very simple strategy based on averaging the observations of multiple interferograms, see Strozzi et al. (2001) and Williams et al. (1998). This last procedure, which is quite popular in literature, is often named interferogram stacking technique.

In this section we describe a procedure based on an adaptive modelling, which fully takes advantage of the correlation properties mentioned in the previous section. The proposed procedure employs a "2.5D modelling", which couples two different models: a 2D model, which is used to assess the subsidence velocity map of the observed field (assuming a constant deformation rate over the observed time interval); and a 1D model, which is employed to estimate the temporal evolution of the subsidence in some selected points of the deformation field. The main features of the proposed procedure are briefly outlined below.

1. The assumption of a constant deformation rate over the observed time interval allows a 2D model to be adopted, instead of a quite more complex 3D one. This assumption should be quite appropriate to different applications (at least as a first approximation).

2. The procedure requires multiple interferograms of the same subsidence area. The interferograms are processed separately, deriving from each interferogram the corresponding velocity field. The velocity fields are then put together as input observations of the 2D estimation procedure (stacked velocity fields). These fields contain the contributions of the four phase components described in the previous section, where in this case  $\Phi_{Mov}$  represents the stationary signal;  $\Phi_{Atm}$  is temporally uncorrelated but can be spatially correlated within each velocity field; and  $\Phi_{Noise}$  and  $\Phi_{Res\_Topo}$  are white noise.
3. The subsidence velocity map is estimated through the classical LS collocation procedure, which involves the estimation of the autocovariance function of the stacked velocity fields, the separation of the signal from the noise (filtering), and the prediction of the signal over location not covered by the input data (Moritz, 1978; Dermanis, 1984). The proposed procedure provides an adaptative filtering, which is only driven by the autocovariance function of the input data, without requiring any explicit modelling of the subsidence at hand: it is quite more flexible than the classical interpolation techniques, e.g. based on polynomials, etc. The collocation filtering may only work if the stationary signal (related to  $\Phi_{Mov}$ ) is "strong enough" to be separated from the  $\Phi_{Atm}$ . This is not the case over the stable areas, which have to be excluded before running the collocation filtering. For this purpose we run a pre-processing of the stacked velocity fields based on a robust filter (a 3D median filtering).
4. The analysis of the temporal evolution of the subsidence is run on the residuals of the 2D collocation filtering (i.e. the differences between the observations and the corresponding estimated signals). Different analysis tools may be implemented: LS linear regression, 1D collocation filtering, etc. In this analysis the data redundancy plays a critical role. In fact, unlike the 2D collocation filtering, where usually large data sets are filtered, this analysis concerns very limited sets of data (say, 15-20 observations, one for each stacked interferogram). In order to gain redundancy, the temporal profiles of neighbour points may be put together. The analysis is typically performed on few selected locations of the deformation field under analysis (for instance, the location of the maximum deformation rate and some points of particular interest). This step is fundamental to check the goodness of the 2D model assumption (constant deformation velocity).

#### 4. DISCUSSION OF THE RESULTS

The performances of the proposed procedure were tested on simulated DInSAR data that roughly reproduce the characteristics of a real subsidence phenomenon: the urban subsidence of Sallent (North Catalunya, Spain), which has been extensively analysed at the Cartographic Institute of Catalonia, see (Crosetto et al., 2002a; Crosetto et al., 2002b). This subsidence, which has slow deformation rate and small spatial extent, represents a quite difficult case for the usage of the DInSAR technique. The simulated data include different components, as it is detailed below.

1. A 3D deformation field,  $d = F(X, Y, t)$ , whose main characteristics, like the shape, extension, deformation rate and temporal evolution, are quite similar to those of the Sallent subsidence. This is an "error-free" field, which was used in the

analysis as a reference to assess the performances of the proposed filters. A deformation map, which corresponds to an observation interval of 5 years, is shown in Figure 2. The maximum deformation rate is 20 mm/yr.

2. A 3D atmospheric field, which reproduces the contribution of the atmospheric effects. This field is spatially correlated, i.e. within a given interferogram (at a fixed  $t$ ) it is correlated in the  $[X, Y]$  domain. The data simulation was originally designed to work in a Monte Carlo framework. Therefore all the data (with the exception of the deformation field) were generated randomly. For each interferogram the generation of the atmospheric fields is based on the Cholesky decomposition, see for instance (Crosetto et al., 2001), and is driven by the standard deviation  $\sigma_{Atm}$  of the atmospheric component and its correlation length  $L_C$ . An example of an atmospheric field is shown in Figure 3. This field covers approximately the same area shown in Figure 2 and has a grid spacing of 20 m. In this case  $\sigma_{Atm}$  is 5.7 mm/yr and  $L_C$  is about 210 m.
3. A 3D white noise field, which includes the contributions of  $\Phi_{Noise}$  and  $\Phi_{Res\_Topo}$ . This field is randomly generated assuming a zero-mean normally distributed noise. For each pixel, the noise standard deviation  $\sigma_{noise}$  is derived from the coherence map of the associated interferogram (for a review of different methods to estimate the phase noise as a function of the coherence, see (Hanssen, 2001)). An example of white noise, which is superposed to a deformation field is shown in Figure 4. This field covers the same area from Figure 3, with a 20-m grid spacing). In this case the average  $\sigma_{noise}$  is 3.4 mm/yr.
4. The unwrapping related errors represent a particular type of errors in the interferometric data. They are due to aliasing effects during the phase unwrapping. Since they are multiple of  $2\pi$  they have a large magnitude compared to the noise. They are usually associated with low coherence areas and affect clusters of neighbour pixels. These errors may be included in the simulated data.
5. The subsidences characterized by slow deformation rates, such as the one considered in this work, are only detectable over large observation intervals, where the SAR images usually have very low coherence. In low coherence areas the phase noise is high and it is often not possible to unwrap the interferometric phase, thus causing a data loss. The data loss was taken into account in the data simulation. An example is shown in Figure 4, where the data loss is 32.6 %.

In order to test the proposed procedure, different data simulations were performed. Firstly, the 2D LS collocation was run on a 3D dataset which consists of 10 stacked velocity fields and which includes the reference deformation field, the white noise and the data loss effect. The autocovariance function of this dataset is shown in Figure 5. The total variance  $\sigma_T^2$  is 47.91 mm<sup>2</sup>/yr<sup>2</sup>, while the variance of the signal is 64.5 % of  $\sigma_T^2$ . The average data loss is 32.6 %. This dataset does not include a temporal evolution of the deformation (i.e. it has a constant deformation rate). In Figure 6 it is shown a profile of the observations (i.e. the input data of the estimation procedure), the estimated deformation field (estimated signal) with the associated confidence bands (signal  $\pm$  standard deviation). The location of

the profile is illustrated in Figure 2. One may notice that the estimated signal follows rather well the reference profile. It is important to note that this last profile was not used in the estimation of the signal. An exception occurs in the left part of the profile, where the reference values have a localized variation: in this case the LS collocation method, due to the structure of the autocovariance function that is reported in Figure 5, does not "recognize" this variation as a signal and therefore performs a smoothing of the surface.

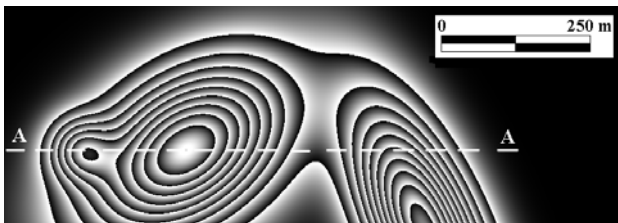


Figure 2. Simulated deformation map, which corresponds to a time interval of 5 years. Each fringe corresponds to a vertical movement of 10 mm.

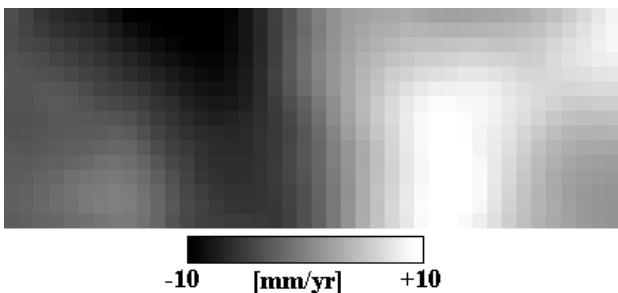


Figure 3. Example of an atmospheric field with 20-m grid spacing, which covers the same area from Figure 2.

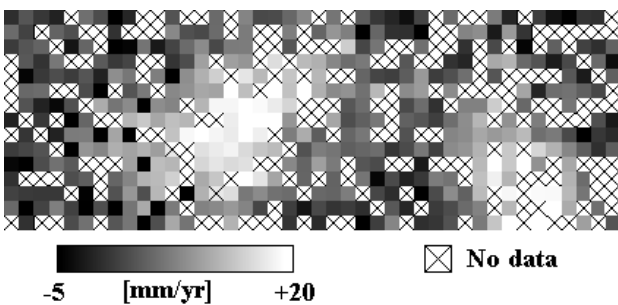


Figure 4. A noise field superposed to a deformation field, which covers the same area from Figure 2. The grid spacing is 20 m; the data loss is 32.6 %.



Figure 5. Autocovariance function of a simulated dataset which consists of 10 stacked velocity fields. The total variance  $\sigma_T^2$  is 47.91 mm<sup>2</sup>/yr<sup>2</sup>; the variance of the signal is 64.5 % of  $\sigma_T^2$ .

A second dataset was generated to check the robustness of the LS collocation method against the "outliers" due to unwrapping related errors. In Figure 7 it is shown a profile of the observations, the estimated signal and its associated confidence band. The noise and data loss were the same as in the previous dataset. The considered cluster of outliers includes 6 by 6 pixels (six of them are visible in the profile) with a magnitude of 30 mm/yr (this corresponds to a phase error of  $2\pi$  for an interferogram with 1-year observation interval). One may notice a localized effect (in the interval between 400 and 520 m) on the estimated signal. However, the maximum amplitude of this effect is less than 3 mm/yr, i.e. less than one tenth of the magnitude of the input errors. The LS collocation method is quite robust against the unwrapping related errors, which can be easily detected and eliminated by analysing the residuals of the LS collocation estimation. This may appropriately be performed using the classical Baarda data snooping (Baarda, 1968).

The filtering of the atmospheric component represents the most delicate step of the proposed procedure. In fact, the LS collocation is only able to filter out the uncorrelated part (noise) of the input observations from their correlated part (signal). As already discussed in the previous section, the collocation filtering is expected to work on a stacked velocity fields if the signal related to  $\Phi_{Mov}$  is enough strong to overcome the signal due to  $\Phi_{Atm}$ . This should reasonably happen because the component due to  $\Phi_{Mov}$  is stationary in time (therefore it has a strong correlation in the stacked velocity fields), while  $\Phi_{Atm}$  is temporally uncorrelated: increasing the number of interferograms implies  $\Phi_{Atm}$  to be considered as a noise component in the stacked signal. We have however to recognize that this is a quite heuristic approach. In practice, given a set of interferograms the strength of the signal due to  $\Phi_{Atm}$  will depend on the magnitude of the atmospheric effects on each interferogram, on their spatial correlation length and on the total number of interferograms.

Two scenarios may be foreseen. In the most favourable one, which is most likely to occur using large numbers of interferograms, the atmospheric effects tend to cancel out in the mean, leaving a weak signal due to  $\Phi_{Atm}$ . In this case the signal estimated with the LS collocation method will be unbiased, or only slightly affected by the atmospheric effects, like in the case

shown in Figure 6. In this case the interferograms affected by severe atmospheric effects may be identified by analysing the residuals of the LS collocations: the corresponding residuals will show a very strong correlation, while in absence of (or with weak) atmospheric effects the residuals will tend to behave as white noise. These interferogram could be eliminated to perform a more refined estimation of the signal (second iteration). What happens in the second scenario, when the atmospheric effects do not cancel out completely? An example, based on simulated data, is shown in Figure 8. A dataset of 10 interferograms was generated, assuming for the atmospheric effects that  $L_C$  is 600 m, and  $\sigma_{Atm}$  is 15 mm/yr and 4.5 mm/yr in the 20 % and 47 % of the

interferograms, respectively. In the remaining 33 %,  $\sigma_{Atm}$  was assumed to be naught (negligible atmospheric effects). In this case, the average of the atmospheric effects is significantly different from zero, see Figure 8: there is a residual trend (from about - 3.5 mm/yr, on the left part of the profile, to 3.6 mm/yr on the right one) that results in a linear bias in the estimated signal. In this case it is not possible to identify the interferogram(s) affected by severe atmospheric effects. In fact, the linear bias in the estimated signal corrupts the residuals of the LS collocation, which will exhibit correlation even if the associated interferograms have no atmospheric effects.

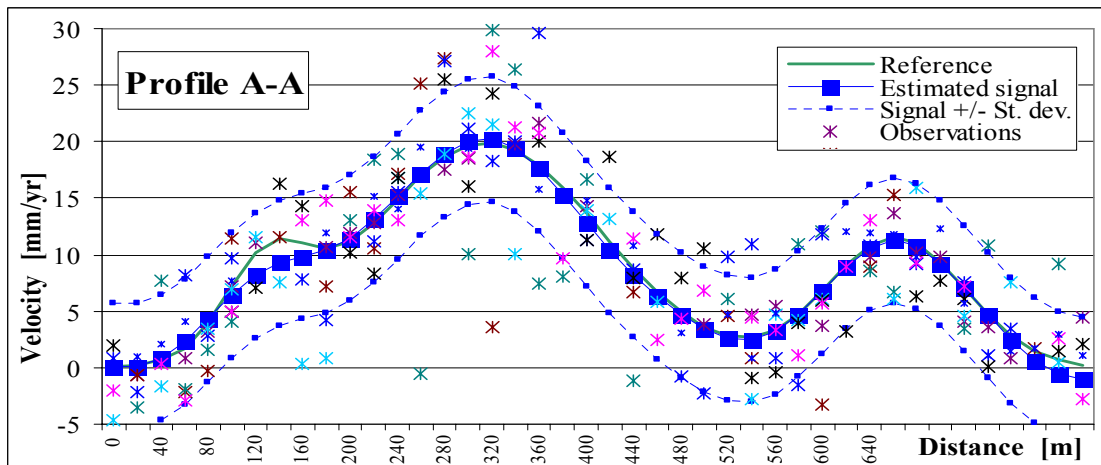


Figure 6. Filtering on a set of 10 stacked velocity fields, which includes white noise and the data loss effect. Profile of the observations and the estimated deformation (estimated signal) with the associated confidence bands (signal  $\pm$  standard deviation).

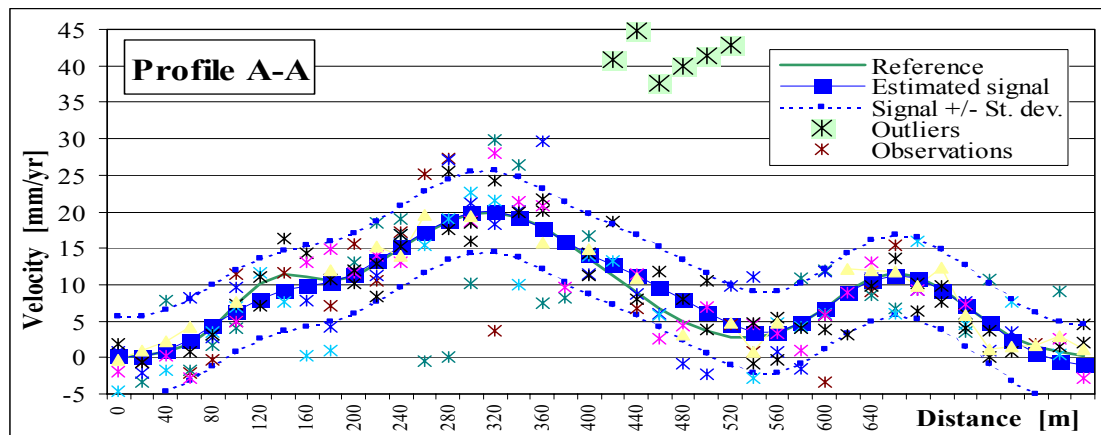


Figure 7. Filtering on a set of 10 stacked velocity fields, which includes outliers due to unwrapping related errors, whose magnitude is 30 mm/yr. The outliers have a localized effect (between 400 and 520 m) on the estimated signal.

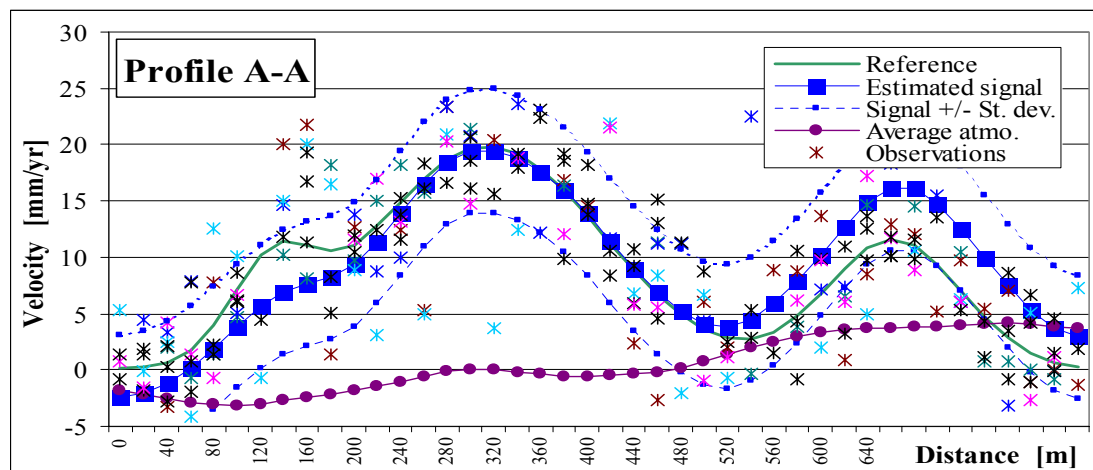


Figure 8. Filtering on a set of 10 stacked velocity fields, which includes atmospheric effects. The temporal average of these effects is significantly different from zero; this results in a residual in a linear bias in the estimated signal.

The possibility to get a biased deformation field due to non-compensated atmospheric effects could represent a limitation of the procedure. It is however important to underline that the above example is based on synthetic data and that the actual possibility to get, in real data, the same residual atmospheric effect has to be assessed by analysing sets of real interferograms over stable areas. The influence of the atmospheric component may be drastically reduced if stable areas can be identified in the vicinity of the deformation area under analysis. In this case, in fact, the procedure described in section 2 may be used to classify, from the viewpoint of atmospheric effects, reliable and potentially degraded interferograms. The latter ones could be eliminated (or under weighted, in case a weighted collocation procedure is used) before running the collocation filtering.

## 5. DISCUSSION AND CONCLUSIONS

In this paper an adaptive modelling, which takes advantage of the properties of multiple DInSAR observations has been described. In the proposed procedure two models are coupled: a 2D model, which is used to assess the velocity map of the observed field, and a 1D model, which is employed to estimate the temporal evolution of the subsidence in some selected points. In this paper the analysis of the results has been only focused on the 2D collocation filtering. The proposed filtering provides a flexible modelling tool for the deformation fields with low spatial frequency characteristics. An important advantage is that it provides the filtered and predicted signals with their associated variances, thus describing the stochastic features of the estimated deformation field. The procedure works properly with quite noisy observations. It accepts in input evenly distributed observations: all the results described in this paper were obtained on irregular grids of data, which include an important percentage of "holes" due to data loss. Furthermore, the procedure is robust against outliers, like those due to unwrapping related errors, which may be easily eliminated by analysing the residuals. The procedure can separate the deformation from the atmospheric component, unless there are strong non-compensated atmospheric effects.

Two future developments of the present work are foreseen: the implementation of a fully 3D modelling, and the fusion of data coming from different sources. The extension from 2D to 3D

would be of particular interest for all the subsidences characterized by important temporal variability. It would require an adequate number of interferograms. In fact, dealing with 3D fields involves a much larger number of unknown in the LS collocation. The data fusion could be used to estimate the deformation fields starting from heterogeneous sources, like DInSAR, GPS, levelling networks, etc. This could be done by using a weighted version of the LS collocation filtering.

## ACKNOWLEDGMENTS

This work has been partially supported by the Spanish Commission for Science and Technology (ICYT) TIC99-1050-C03-03.

## REFERENCES

- Amelung F., Galloway D.L., Bell J.W., Zebker H.A., Lacznik R.J., 1999. Sensing the ups and downs of Las Vegas: InSAR reveals structural control of land subsidence and aquifer-system deformation. *Geology*, Vol. 27, No. 6, pp. 483-486.
- Amelung, F., Jonson S., Zebker H.A., Segall P., 2000. Widespread uplift and 'trapdoor' faulting on Galápagos volcanoes observed with radar interferometry. *Nature*, Vol. 407, pp. 993-996.
- Baarda W., 1968. A testing procedure for use in geodetic networks. *Netherlands Geodetic Commission – Publications on Geodesy*, Vol. 2, No. 5, Delft (Holland).
- Berardino P., Fornaro G., Fusco A., Galluzzo D., Lanari R., Sansosti E., Usai S., 2001. A new approach for analysing the temporal evolution of earth surface deformations based on the combination of DIFSAR interferograms. *Proceedings of IGARSS 2001*, Sidney (Australia).
- Carnec C., Massonnet D., King C., 1996. Two examples of the use of SAR interferometry on displacement fields of small spatial extent. *Geophysical Research Letters*, Vol. 23, No. 24, pp. 3579-3582.

Crosetto M., Moreno Ruiz J.A., Crippa B., 2001. Uncertainty propagation in models driven by remotely sensed data. *Remote Sensing of Environ.*, Vol. 76, No. 3, pp. 373-385.

Crosetto M., Tscherning C.C., Crippa B., Castillo M., 2002a. Subsidence Monitoring using SAR interferometry: reduction of the atmospheric effects using stochastic filtering. *Geophysical Research Letters*, Vol. 29, No. 9.

Crosetto M., Castillo M., Arbiol R., 2002b. Urban subsidence monitoring using radar interferometry: Algorithms and validation. Submitted to *Photogramm Eng Rem Sens*.

Dermanis A., 1984. Kriging and collocation: a comparison. *Manuscripta Geodaetica*, Vol. 9, No. 3, pp. 159-167.

Ferretti A., Prati C., Rocca F., 2000. Nonlinear subsidence rate estimation using permanent scatterers in differential SAR interferometry. *IEEE Transactions on Geoscience and Remote Sensing*, Vol. 38, No. 5, pp. 2202-2212.

Goldstein R.M., Englehardt H., Kamb B., Frolich R.M., 1993. Satellite radar interferometry for monitoring ice sheet motion: application to an Antarctic ice stream. *Science*, Vol. 262, pp. 1525-1530.

Hanssen R., 2001. *Radar interferometry*. Kluwer Academic Publishers, Dordrecht, The Netherlands.

Kwok R., Fahnestock M.A., 1996. Ice sheet motion and topography from radar interferometry. *IEEE Transactions on Geoscience Remote Sens.*, Vol. 34, No.1, pp. 189-200.

Lu Z., Danskin W.R., 2001. InSAR analysis of natural recharge to define structure of a ground-water basin, San Bernardino, California. *Geophysical Research Letters*, Vol. 28, No. 13, pp. 2661-2664.

Massonnet D., Rossi M., Carmona C., Adragna F., Peltzer G., Feigl K., Rabaute T., 1993. The displacement field of the Landers earthquake mapped by radar interferometry. *Nature*, Vol. 364, pp.138-142.

Massonnet D., Feigl K., Rossi M., Adragna F., 1994. Radar interferometry mapping of deformation in the year after the Landers earthquake. *Nature*, Vol. 369, pp. 227-230.

Massonnet D., Briole P., Arnaud A., 1995. Deflation of Mount Etna monitored by spaceborne radar interferometry. *Nature*, Vol. 375, pp. 567-570.

Moritz H., 1978. Least-squares collocation. *Rev. Geophys. Space Phys.*, Vol. 16, pp. 421-430.

Strozzi T., Wegmüller U., Tosi L., Bitelli G., Spreckels V., 2001. Land Subsidence Monitoring with Differential SAR Interferometry. *Photogrammetric Engineering and Remote Sensing*, Vol. 67, No. 11, pp. 1261-1270.

Williams S., Bock Y., Fang P., 1998. Integrated satellite interferometry: Tropospheric noise, GPS estimates and implications for interferometric synthetic aperture radar products. *Journal of Geophysical Research*, Vol. 103, B11, pp. 27051-27067.

